Strategies to improve the photochromic properties and photovoltaic performances of naphthopyran dyes in dye-sensitized solar cells

Valid Mwalukuku, Johan Liotier, Antonio J. Riquelme, Yann Kervella, Quentin Huaulmé, Alix Haurez, Stéphanie Narbey, Juan Antonio Anta, Renaud Demadrille

Strategies to improve the photochromic properties and photovoltaic performances of naphthopyran dyes in dye-sensitized solar cells.

*Valid M. Mwalukuku, Johan Liotier, Antonio J. Riquelme, Yann Kervella, Quentin Huaulmé, Alix Haurez, Stéphanie Narbey, Juan Antonio Anta, and Renaud Demadrille**

This work is dedicated *in memoriam* to the late Prof. M. Campredon who passed away in 2022.

V. M. Mwalukuku, Dr. J. Liotier, Y. Kervella, Dr. Q. Huaulmé, A. Haurez,
Dr. R. Demadrille
Univ. Grenoble Alpes, CNRS, CEA, SyMMES, 17 rue des martyrs, 38000 Grenoble, France
E-mail: renaud.demadrille@cea.fr

S. Narbey
Solaronix SA, Rue de l'Ouriette 129, 1170 Aubonne, Switzerland.

Dr. A. J. Riquelme, Prof. J. A. Anta
Área de Química Física, Universidad Pablo de Olavide, E-41013 Seville, Spain

Keywords: photochromic, photovoltaic, dye-sensitized solar cells, semi-transparent solar cells

Abstract:

Semi-transparent solar cells are emerging as promising devices for building integrated photovoltaics. However, regardless of the technology considered, the optical transmission of semi-transparent solar cells is fixed during the fabrication process, and hence, cannot adjust to variations in daylight or weather conditions. This becomes an issue when applications such as photovoltaic windows are envisioned. Previously, we have reported that the use of photochromic naphthopyran dyes in dye-sensitized solar cells (DSSC) allows for the fabrication of semi-transparent devices capable of modulating their light transmission and energy production depending on light intensity. Herein, we report a series of naphthopyran dyes with an identical pi-conjugated backbone and varying alkyl substituents. Using this molecular engineering strategy, we demonstrate control of the discoloration kinetics of the photochromic dyes and the reduction of undesirable recombination processes when utilised in solar cells. We

establish clear photochromic-photovoltaic structure-property relationships for these new photosensitizers and demonstrate improved photovoltaic performances and photochromic responses in DSSC with notably faster discoloration than previously reported. We also explore, for the first time with photochromic molecules, the co-sensitization of the electrodes and report the highest power conversion efficiency for a photochromic DSSC, reaching up to 4.34% under standard conditions.

1. Introduction

In 2004, Nobel Laureate Richard Smalley stated: "energy is the most important problem facing humanity today". Eighteen years later, this problem has still not been solved, and has been worsened by climate change linked to the over-reliance on fossil fuels. As a result, as of today, it is crucial to increase our exploitation of renewable energy sources using technologies that limit/reduce/minimise the emission of greenhouse gas emissions. To address this problem, considerable research has been conducted in the last two decades, with a large focus on solar energy conversion. Solar energy is a valuable source to reduce the carbon footprint of the energy production, and it appears indispensable if we are to meet the ever-increasing energy demand of our modern society. Recently, new solar cell technologies, based on not only cheap and abundant materials but also low-cost and industrially compatible manufacturing methods have emerged. These technologies include perovskite solar cells (PSC), organic solar cells (OPV) and dye-sensitized solar cells (DSSC).[1] The performances of these last generations of photovoltaic devices have been strongly improved and today, certified power conversion efficiencies of over 25.7% for PSCs[2], over 18.7% for OPVs[3] and over 13% for DSSCs[4] have been reported.[5] One unique feature of this latest generation of solar cells is that they are fully customizable and can be designed as semi-transparent. Semi-transparent devices are interesting because they do not only generate electricity, but they also have aesthetic and functional advantages particularly appealing for large-scale integration on facades and roofs of buildings[6], greenhouses[7], as well as in transport vehicles.[8] As a result, it can be predicted that translucent solar cells will probably provide a valuable complementary technology to traditional photovoltaic technologies for reducing the carbon footprint of buildings and converting them into power plants in the future.[9]

However, semi-transparent solar cells yield an inherently poorer performance than their opaque counterparts since they only convert a lower fraction of the incident photons.[10] Additionally, in order to integrate them into building facades as windows, they have to be highly translucent;

thus, a compromise between transparency and efficiency must be found. Nonetheless, regardless of technology utilised, semi-transparent solar cells possess an optical transmission that is chosen and fixed during the manufacturing process.[11]–[15] This invariable light transmittance can be problematic for photovoltaic windows under variable weather and light conditions, where, to achieve the level of transparency necessary for the users' comfort in any light conditions, the efficiency of these solar cells has often to be sacrificed. Several strategies have been developed in the last years to improve the transparency of translucent solar cells while maintaining an acceptable efficiency. One example is the development of photoactive materials with selective absorption in the near infrared (NIR)[16][17] or the UV range.[18] Our approach to tackle this challenge is different. We recently discovered that the use of photochromic naphthopyran dyes as photosensitizer in DSSCs is a promising approach to obtain semi-transparent solar cells with light-driven and self-adjustable optical properties.[19] In 2020, we reported **NPI**, a push-pull diphenyl-naphthopyran dye, allowing for the fabrication of semi-transparent photochromic DSSCs and mini-modules. **NPI** exhibits an extended pi-conjugated photochromic unit based on an indeno-fused moiety, essential to shift the absorption spectrum of the uncoloured closed form above 400 nm.[20] The CF form weakly absorbs in the visible because the two parts of the molecule, *i.e.* the one bearing the donating unit and the one bearing the accepting anchoring unit are not conjugated. Upon absorption of a photon, the carbon-oxygen bond of the pyran ring undergoes a homolytic cleavage. After rearrangement of the pi-conjugated system, a fully conjugated species is formed in which and ICT (internal charge transfer) absorption band appears. This results in an intense absorption of the open form across the visible range after photo-isomerization, giving a deep green coloration at the photostationary state (PSS). Furthermore, we have demonstrated that when **NPI** is incorporated in a DSSC, the device can switch from a non-coloured state to a coloured state, and consequently, the solar cells could vary their average visible transmittance from 59% to 27%, exhibiting a power conversion efficiency of up to 3.7%. Furthermore, we also demonstrated that the process of coloration-discoloration is fully reversible. Unfortunately, the discoloration of the devices is slow, and the cells recover their initial transparency only after 16h in the dark. In parallel, we were able to show that the photo-isomerization process of the photochromic dye on the surface of the photoanode was responsible for an increased recombination rate of the photo-injected electrons in the TiO_2 with the redox mediator of the electrolyte. However, this leads to a drop of the V_{oc} upon activation of the dye, which is detrimental to the photovoltaic performances.

To account for these two problems, in this work, we explore several modifications of **NPI**'s molecular structure. Molecular engineering was performed through the introduction of various alkyl substituents on the molecule keeping the pi-conjugated backbone identical. Utilising this strategy, we show that thermal discoloration kinetics of the photochromic dyes can be modulated and that the undesirable recombination processes in solar cells can be reduced simultaneously. We establish clear structure-property relationships for this family of photochromic photosensitizers. Small signal perturbation techniques such as electrochemical impedance spectroscopy (EIS) were employed to understand precisely the operation of these new molecules in devices and how the structure modification affects the recombination process. We also explore in this work for the first time, the co-sensitization approach of the electrodes with photochromic dyes and disclose the highest power conversion efficiency ever obtained for a photochromic dye solar cell, reaching 4.34% under standard conditions. We demonstrate for this new generation of solar cells improved photochromic responses with notably faster discoloration kinetics compared to the ones reported in our previous work.

2. Results and discussion

2.1. Molecular design and synthesis of the new dyes

Although several studies have previously been published on the structure-property relationships of diphenyl-naphthopyran photochromic dyes[21]–[24], they were mostly limited to variations of the pi-conjugated structure.[25]–[27] To the best of our knowledge, there is no previous work especially aimed at understanding how non-conjugated substituents can influence the photochromic behaviour of diphenyl-naphthopyran dyes. Based on our previous work, we started from the molecule coded **NPI** and introduced alkyl substituents in various positions. Alkyl substituents were attached either on the indeno bridge of the photochromic core or the diphenylamine (DPA) unit, resulting in the preparation of five new naphthopyran derivatives. Modification of the photochromic core is expected to affect the discoloration kinetics, whereas the introduction of alkyl chains on the electron-donating part is expected to shift the absorption toward the visible range[28], and help cushioning the TiO_2 from the oxidized species in the electrolyte consequently reducing the recombination processes.[29]

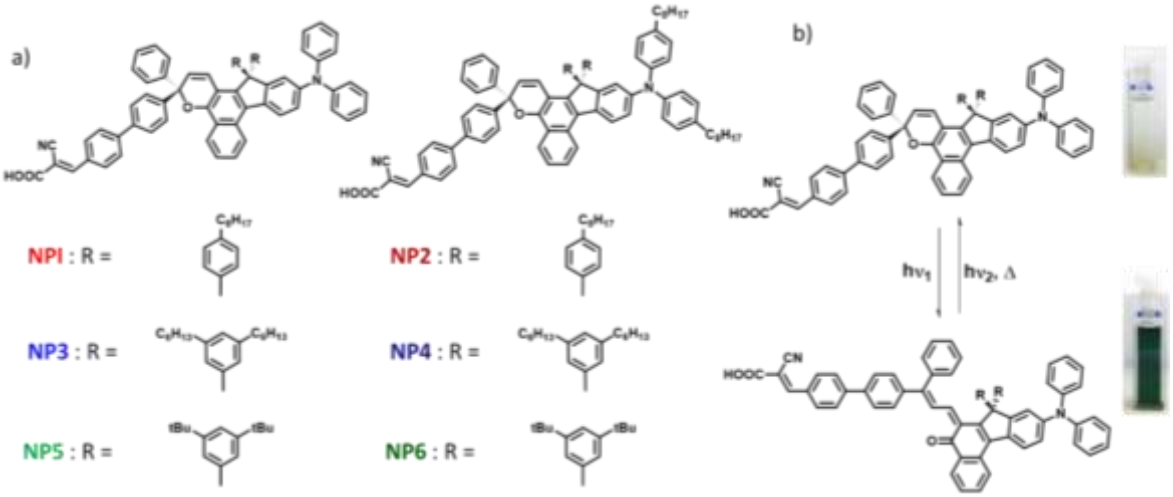

Figure 1: a) Chemical structures of **NPI** (reference dye) and the 5 new dyes synthesized and studied in this work (**NP2** to **NP6**), b) Scheme of the photochromic interconversion from the closed form (CF) to the open form (OF) of **NPI** representative for this class of compounds.

As shown in **Figure 1**, the chemical structure of **NP2** was derived from the one of **NPI** dyes/from the NPI dye, where the only difference is the introduction of *n*-octyl chains at the periphery of the DPA donor unit. **NP3** and **NP5** differ from **NPI** by the introduction of *n*-hexyl and *ter*-butyl groups on the phenyl units that are attached on the central indeno bridge. **NP4** and **NP6** are analogs of **NP3** and **NP5** respectively with additional *n*-octyl chains on the DPA unit. The synthetic strategy and conditions to prepare the dyes are reported in **Figure 2** and described in detail in section I of the ESI.

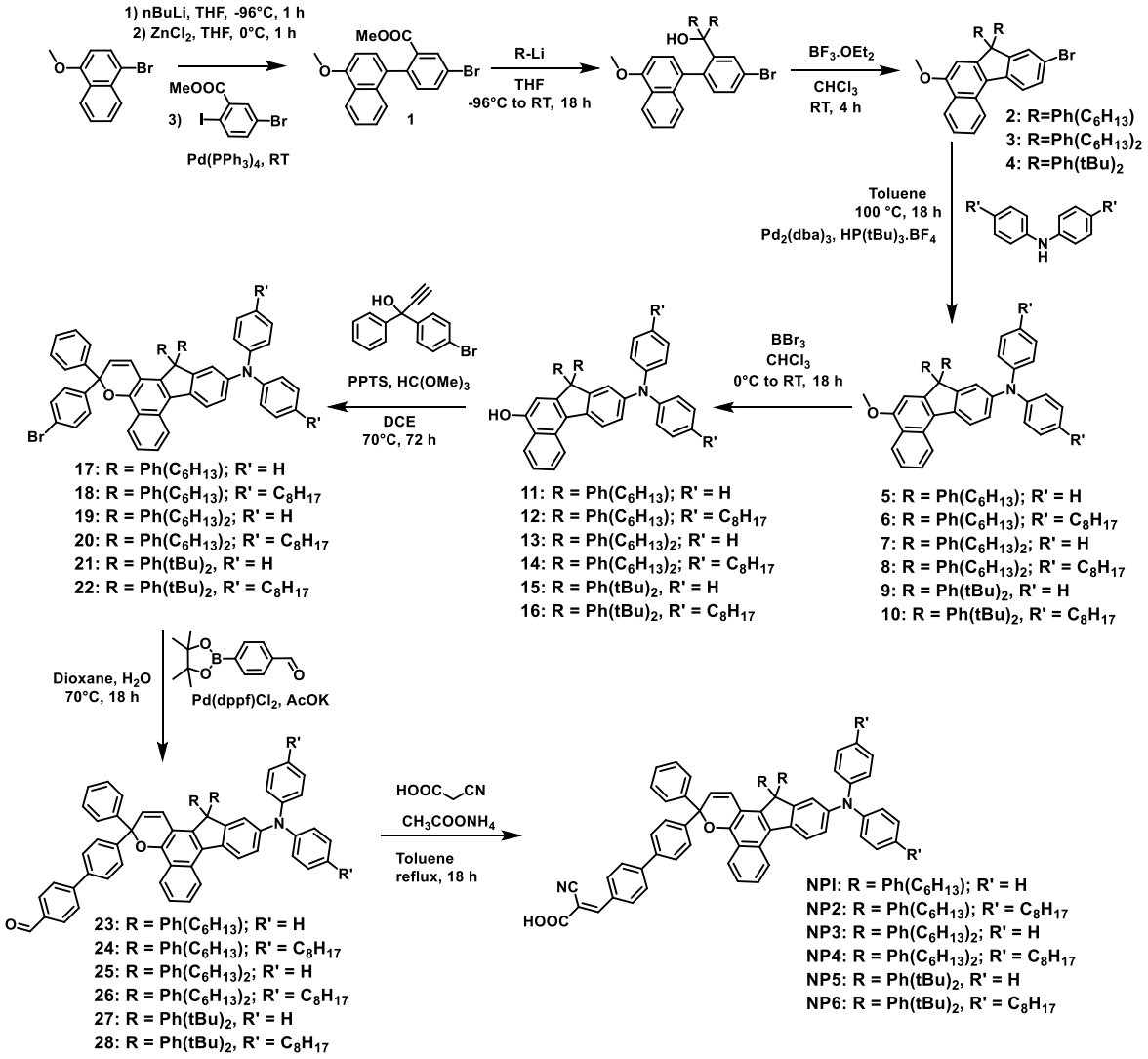

Figure 2: Synthetic pathway to obtain **NPI** to **NP6** dyes

The synthesis of the dyes starts with a Negishi cross-coupling reaction between 1-bromo-4-methoxy-naphthalene and methyl-5-bromo-2-iodobenzoate yielding methyl 5-bromo-2-(4-methoxynaphthalen-1-yl)benzoate (1), a key building block which is common to all the dyes. This precursor is subsequently reacted with lithiated aryls, substituted with the different alkyl groups that we want to introduce, to undergo a nucleophilic addition on the carboxylate unit. The resulting alcohol is cyclized through an intramolecular Friedel-Crafts acylation to produce the methoxy-protected brominated indeno-naphthalene intermediates (compounds **2**, **3**, **4**). A Buchwald-Hartwig cross-coupling reaction is then performed using diphenylamine or bis-(4-octylphenyl)amine to obtain compounds **5**, **7** and **9** or compounds **6**, **8** and **10** respectively. The methoxy protection is easily removed with a BBr_3 solution to resulting in the compounds **11** to **16**. The formation of the naphthopyran ring is then performed by condensation and Claisen rearrangement with 1-(4-bromophenyl)-1-phenylprop-2-yn-1-ol, using pyridinium para-

toluene sulfoxide (PPTS) as weak acid to produce compounds **17** to **22**. This acid was selected to avoid the degradation of the propargylic alcohol via the Meyer-Schuster rearrangement that would lead to a non-reactive cinnamaldehyde derivative. The obtained brominated naphthopyrans are then coupled with 4-(4,4,5,5-tetramethyl-1,3,2- dioxaborolan-2-yl)-benzaldehyde through a Suzuki cross-coupling reaction to yield compounds **23** to **28**. Finally, we obtained the dyes after a Knoevenagel reaction, using ammonium acetate in toluene followed by a purification step via column chromatography, in rather good yields ranging from 45 to 90%. More details can be found in the ESI.

2.2. Optical and photochromic properties of the dyes in solution

The optical and photochromic properties of the dyes were analysed by UV–vis spectroscopy in toluene solution at a concentration of 2×10^{-5} M both in the dark and under illumination using a polychromatic light source (irradiation: 200 W, 300–600 nm). Under these testing conditions, toluene is sufficiently stable to allow the dyes reaching the photostationary state without any degradation. In **Figure 3,** we present and compare the normalized absorption spectra of the closed and opened form isomers and the main optical parameters are given in **Table 1**. Additional information on the optical and photochromic properties and kinetics of each dye can be found in Section II of ESI. The new compounds show a photochromic behaviour similar to **NPI** in solution. Upon irradiation, the homolytic cleavage of the C-O bond of the pyranic ring followed by the rearrangement of the pi-conjugated system leads to the formation of diene coloured isomers that absorb intensively in the visible range up to around 730 nm.

The spectra of the dyes (closed forms, CF) before irradiation are quite similar; they show an absorption limit close to 450 nm making it possible to induce photochromism using high-energy visible photons, which is an advantage for use in solar cells since the TiO_2 film screens most of the UV photons. From the absorption spectra of the CF in solution, it can be concluded that the introduction of alkyl groups on various positions of the photochromic dye have a minor influence on their absorption in the UV range as expected. All the compounds show molar absorption coefficient of the closed form comprised between 35,000 and 44,000 $mol\times L^{-1}\times cm^{-1}$, with **NP2** showing the highest value of 43,790 $mol\times L^{-1}\times cm^{-1}$ in the dark.

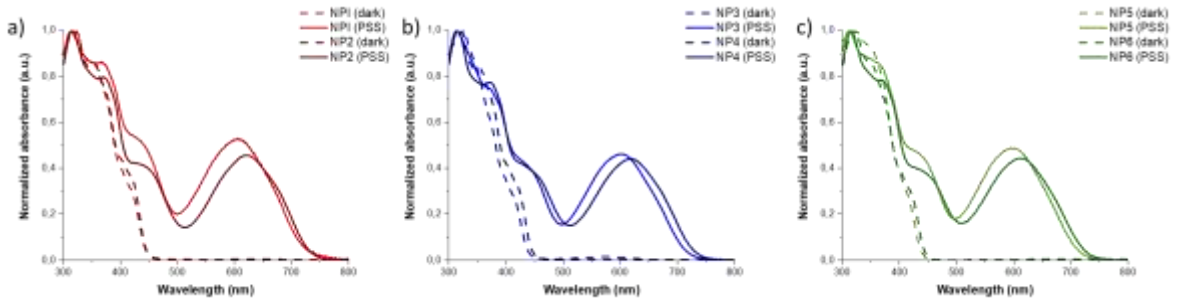

Figure 3: Absorption spectra of the closed form (CF and open form (OF) of a) **NPI** and **NP2**, b) **NP3** and **NP4** and c) **NP5** and **NP6** in their closed forms (dashed curves) and open forms (solid curves) at 25°C, 10^{-5} M (irradiation conditions : 200W Xenon lamp, 300-600 nm filter) in toluene.

Upon irradiation of the dyes with polychromatic light, the absorption spectra of the opened forms (OF) reveal two types of transitions. The peak located around 450 nm likely corresponds to π- π* transitions arising from better conjugation within the open form isomers. Whereas, the intense band that arises at longer wavelengths corresponds to the internal charge transfer (ICT) transition. Minor variations of the spectra are observed corresponding to electronic or steric effects. Notably, the introduction of the octyl chains on the DPA produces a bathochromic shift of around 15 nm compared to the analogue compounds that do not possess those chains on the DPA.

The introduction of bulky substituents (either hexyl or tert-butyle groups) on the indeno bridge has the opposite effect leading to a light hypsochromic shift of the absorption maximum going from 606 nm for NPI to 603 nm for NP3 and to 597 nm for NP5. The same trend is observed going from NP2, to NP4 and NP6. The absorption onsets of all dyes are within the 715-730 nm range. Thus, the optical bandgaps of the OFs are quasi-similar, around 1.7 eV, confirming that chemical modification is not altering significantly the light absorption properties of the dyes.

The discoloration kinetics were analysed by irradiating the dyes until the PSS was reached and then stopping the illumination, leaving the molecules to relax to the closed form in the dark. It is found that in all cases the absorption decreases mono-exponentially according to Equation (1) below. The discolouration curves are reported in **Figure 4**.

Equation (1) : $$A(t) = a_n e^{-k_n t} + A_\infty \quad (1)$$

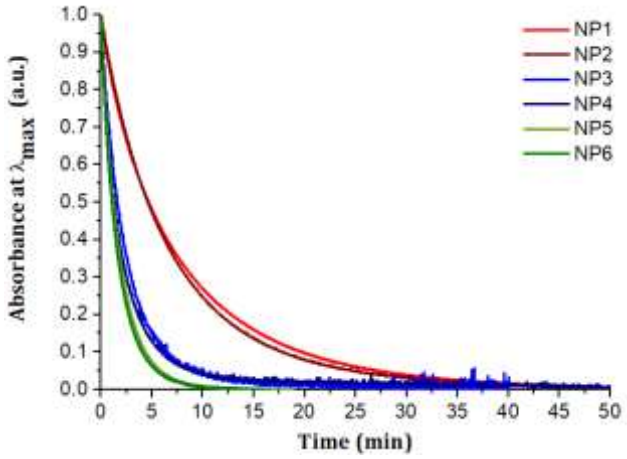

Figure 4: Comparison of normalized discolouration curves of **NPI**-**NP6** in solution after reaching PSS. Conditions 25°C, 10^{-5} M in Toluene.

These curves were modelled using Equation 1, where, $A(t)$ is the absorbance of the sample, k_n is the thermal decolouration kinetic constant (in s^{-1}) of the n^{th} kinetic process, a_n the amplitude of the kinetics of this process, and A_∞ the residual absorbance. The extracted values are reported in **Table 1**.

Dyes	λ_{max} CF (nm)	λ_{onset} CF (nm)	$\varepsilon\ \lambda_{max\ (UV)}$ CF ($mol \times L^{-1} \times cm^{-1}$)	λ_{max} OF (nm)	λ_{onset} OF (nm)	ΔE_{opt} OF (eV)	A_{eq}	k (s^{-1})
NPI	318	450	41 800	606	728	1.70	0.38	2.1×10^{-3}
NP2	320	450	43 790	620	730	1.70	0.38	2.3×10^{-3}
NP3	324	450	35 320	603	716	1.73	0.38	6.3×10^{-3}
NP4	319	450	38 760	617	730	1.70	0.38	7.3×10^{-3}
NP5	324	450	42 310	597	716	1.73	0.38	8.9×10^{-3}
NP6	322	450	40 270	614	729	1.70	0.38	9.7×10^{-3}

Table 1: Optical properties of the six dyes. ΔE_{opt} OF corresponds to the optical bandgap of the opened form; k is the kinetic constant of the mono-exponential modelling of the discoloration curves, A_{eq} corresponds to the absorption intensity observed at the PSS and A_{eq} is optical density of the absorption obtained at PSS.

The effect of the substitution with alkyl groups on the thermal kinetics of decolouration is more significant than on the absorption spectra.. Firstly, comparing **NPI** and **NP2** we can see that the C_8 alkyl chains on the periphery tend to accelerate the thermal decolouration. More strikingly, the kinetics of discoloration are accelerated with increasing the bulkiness of the substituents on the indene group, as shown in **Figure 4**. Indeed, **NPI** and **NP2** have a comparable discolouration constant, whereas, **NP3** and **NP4** discolour three times faster compared to **NPI** and finally **NP5**

and **NP6** solutions can recover their initial transparency more than four times faster than **NPI**. Clearly, the addition of bulky groups on the indene bridge of the photochromic core contributes more to faster recovery of the initial transparency than on the electron-donating TPA unit, where thesteric hindrance prevents the formation of more thermally stable open isomers.[30][31] Indeed, it is known that trans-cis coloured isomers (TC) could upon prolonged irradiation, evolve into more stable trans–trans open isomers (TT) responsible for a persistent coloration.[32][33] These results prove that the strategy of increasing the bulkiness of the substituents attached on the indene unit is a powerful and efficient method to control the kinetics of decolouration without altering the colourability at the PSS.

2.3. Energetic levels of the dyes in their different states

Next, the HOMO-LUMO energy levels of the **NP** dyes were estimated in solution to check whether their positioning matches the DSSC components for electron transfers. We evaluated the energy levels of the frontier orbitals by cyclic voltammetry in dichloromethane before and after irradiation. The cyclic voltammetry carried out yielded values reported in the **Supplementary Figure 19**.

As we have already demonstrated for other diphenyl-naphthopyran molecules, the photo-isomerisation process insignificantly affects the HOMO energy levels , which lie between -5.1 eV and -5.3 eV and are sufficiently high enough to allow for the dyes regeneration process by the I^-/I^-_3 redox couple (-4.9 eV).[34] The LUMO levels are more significantly altered by the photo-isomerisation with a downshift of 0.5-1.0 eV induced by the pyran ring opening and the formation of the ketone. However, the LUMO levels are still high enough to allow the electronic transfer into the conduction band (CB) energy level of TiO_2 metal oxide (-4.1 eV).[35][36] Despite this modification of the energetic levels upon isomerization, their energetic positions in all conformations remain favourable to be used in a DSSC configuration.[19]

2.4. Interplay between photochromic and photovoltaic performances

2.4.1. Effect of the substitution of dyes on the J_{sc} and photovoltaic performances

We evaluated the photovoltaic performances of the new photochromic photosensitizers and compared them to the ones of **NPI,** our reference dye, by fabricating opaque and semi-transparent DSSCs. For comparison purposes, all the dyes were tested with identical device configurations. We recorded the current-voltage characteristics at different time intervals of

exposure to light (standard irradiation AM1.5G at 1000 $W \times m^{-2}$) until the cells reached the photostationary state (PSS). The PV parameters *i.e* the short-circuit current density (J_{sc}), open-circuit voltage (V_{oc}), fill factor (FF), and power conversion efficiency (PCE) were extracted from the current-voltage curves. All experimental details related to the fabrication and characterization of the devices are available in Section III of ESI. TiO_2 mesoporous electrodes were composed of a 13 µm-thick transparent layer for semi-transparent devices, and for the opaque cells, the transparent electrodes were covered by a 3 µm-thick scattering layer. We used a homemade electrolyte that we previously developed for **NPI**-based solar cells (90 mM I_2 and 0.5M LiI in acetonitrile), in which, we removed *tert*-butyl pyridine to guarantee that the energy offset between the LUMO of the dyes and the conduction band (CB) of the oxide is high enough to permit the efficient electron injection.

It is well established that the dye adsorption on TiO_2 surface could result in unfavourable aggregation, thus lowering the performance.[37] The use of a co-adsorbent such as chenodeoxycholic acid (CDCA) or derivatives[38] is useful to prevent this phenomenon.[39][40] Whilst the bulkiness of some of the substituents attached to the new dyes could prevent their aggregation, it is important to determine if the use of CDCA as an additive in the manufacturing of the device is required. We compared the resulting photovoltaic parameters of devices sensitized without CDCA to solar cells sensitized with different concentrations of CDCA. **Supplementary Table 3** shows the role played by CDCA on the photovoltaic performances of the photochromic DSSCs. When electrodes were sensitized without CDCA, we observed systematically lower performances, therefore, despite the substitution of bulky groups on the **NP** dyes, CDCA probably contributes to reduce further the formation of aggregates. Besides, additives are also known to fill free spaces between the dyes at the semi-conductor's surface, thus also playing a role on the recombination processes.[40][41]

Then, the photovoltaic performances of the **NP** series dyes were evaluated after incorporation in opaque and semi-transparent DSSC configurations. We used the same batch of electrodes, and the **NP**:CDCA mole ratio was fixed at 1:5 for comparison purposes. Under these conditions, we could accurately compare the photochromic behaviour and the performances of the dyes.

These results are reported in **Table 2**, where the electrical parameters of the best devices based on opaque or transparent electrodes are given, followed by their statistics in parentheses. Finally, the dye loading was measured for all dyes. All the dyes in this family behaved similarly, including a moderate photovoltage and the increase in J_{sc} with irradiation time.

Dyes	Electrode	Jsc ($mA \times cm^{-2}$)	Voc (V)	FF	PCE (%)	Dye Loading ($moles \times cm^{-2}$)
NP1	Transparent	10.45 (10.27 ± 0.29)	0.522 (0.525 ± 0.003)	0.660 (0.652 ± 0.019)	3.59 (3.52 ± 0.05)	1.83×10^{-7}
	Opaque	11.04 (10.74 ± 0.21)	0.535 (0.531 ± 0.008)	0.657 (0.677 ± 0.014)	3.89 (3.83 ± 0.04)	1.98×10^{-7}
NP2	Transparent	12.90 (12.62 ± 0.52)	0.492 (0.484 ± 0.012)	0.615 (0.612 ± 0.016)	3.90 (3.73 ± 0.17)	1.47×10^{-7}
	Opaque	12.74 (13.55 ± 0.67)	0.503 (0.491 ± 0.009)	0.649 (0.620 ± 0.020)	4.16 (4.12 ± 0.04)	2.15×10^{-7}
NP3	Transparent	7.44 (6.85 ± 0.66)	0.555 (0.544 ± 0.007)	0.712 (0.711 ± 0.004)	2.94 (2.65 ± 0.28)	1.61×10^{-7}
	Opaque	8.85 (8.39 ± 0.40)	0.548 (0.555 ± 0.007)	0.699 (0.704 ± 0.004)	3.39 (3.27 ± 0.09)	1.74×10^{-7}
NP4	Transparent	9.17 (9.01 ± 0.15)	0.529 (0.532 ± 0.004)	0.670 (0.673 ± 0.003)	3.26 (3.22 ± 0.02)	1.35×10^{-7}
	Opaque	9.77 (9.51 ± 0.26)	0.546 (0.545 ± 0.003)	0.716 (0.721 ± 0.008)	3.82 (3.74 ± 0.05)	1.37×10^{-7}
NP5	Transparent	5.78 (5.50 ± 0.24)	0.544 (0.548 ± 0.002)	0.734 (0.736 ± 0.004)	2.31 (2.22 ± 0.07)	1.30×10^{-7}
	Opaque	6.23 (5.97 ± 0.24)	0.550 (0.554 ± 0.008)	0.731 (0.732 ± 0.000)	2.50 (2.42 ± 0.06)	1.28×10^{-7}
NP6	Transparent	8.31 (7.69 ± 0.70)	0.482 (0.496 ± 0.014)	0.676 (0.691 ± 0.018)	2.70 (2.62 ± 0.10)	1.14×10^{-7}
	Opaque	9.61 (9.27 ± 0.37)	0.500 (0.506 ± 0.008)	0.674 (0.685 ± 0.010)	3.24 (3.21 ± 0.03)	1.13×10^{-7}

Table 2: Photovoltaic parameters of the optimized solar cells fabricated with opaque (13 µm mesoporous + 3 µm scattering layer) and transparent (13 µm mesoporous) electrodes from the same batch under irradiation AM1.5G at 1000 $W \times m^{-2}$. The Dye:CDCA mole ratio was set to 1:5 for comparison purposes. Statistical data was obtained for at least 3 cells.

To begin with, we analyzed the effect of the introduction of alkyl chains on the DPA. With classical dyes, the introduction of alkyl chains on the electron-donating unit often prevents the redox mediator in the electrolyte from reaching the TiO_2. This inhibits the recombination of electrons and improves the photovoltage and photocurrent. With **NP2**, we wanted to verify if a similar effect could be demonstrated with photochromic dyes. When comparing **NPI**- and **NP2**-based solar cells, it is clear that the introduction of octyl chains is beneficial to the PV performances. The mean PCE values rise from around 3.5% to 3.7% for the semi-transparent solar cells and from 3.8% to 4.1% for the opaque ones, where theimprovement of the performances is linked to an increase of the J_{sc}. For instance, in transparent solar cells, **NP2** gives a quite high J_{sc} of 12.90 $mA \times cm^{-2}$ whereas **NPI** shows a J_{sc} of 10.45 $mA \times cm^{-2}$ despite the dye loading is quite comparable for both dyes. The same observation applies to the opaque solar cells. Interestingly, the beneficial effect of the introduction of the octyl chains can be confirmed by the other dyes. **NP4** and **NP6** show higher performances compared to their respective analogues **NP3** and **NP5** and once again, the increase in J_{sc} is responsible for the improvement of the PCE. This increase in J_{sc} can be attributed, at least partially, to the red-shifted absorption spectra of the dyes bearing octyl chains. The incident photon to current efficiency (IPCE) spectra included in the ESI confirms this observation and demonstrate that both the coloured and non-coloured isomers can generate the current. The bandgaps of the solar cells before and after activation extracted from the IPCE spectra[42] are also given in ESI.

Unfortunately, the introduction of the alkyl groups on the DPA also induces a light drop of the V_{oc} measured at PSS. The evolution of the V_{oc} when the cells are exposed to a prolonged irradiation will be discussed further later.

Secondly, we analysed the effect of the bulky groups introduced on the indene bridge. **NP3** and **NP5** dyes, bearing, respectively, four hexyl and tert-butyl chains, were designed to study how the steric hindrance influences on the speed of decolouration[24] and the PV performance of the photochromic DSSCs. When comparing their PCE to that of **NPI**, it it can be clearly observed that the introduction of four alkyl chains (linear or ramified) on the *meta* position of the phenyl groups attached on the indene bridge is detrimental to the performance. The **NP3**-opaque cell exhibits a J_{sc} of 8.85 mA×cm^{-2} and the **NP5**-opaque cell exhibits a J_{sc} of 6.23 mA×cm^{-2}. This corresponds to a drop of *circa* 20% and 40% of the $J_{sc,}$ respectively. However, we observe that the V_{oc} obtained at PSS is slightly improved for **NP3** and **NP5**. Unfortunately, this does not compensate for the large decrease in J_{sc} and overall, the PCE are severely impacted. The same trend is observed in semi-transparent cells.

Again, the findings can be extended to analogues of **NPI**, **NP3** and **NP5** bearing octyl groups on the DPA. We can see that the PCE of **NP4** and **NP6** decrease compared to **NP2** in both opaque and semi-transparent cells where the reason for this is again a drop in J_{sc}. Since the dye-loading values measured for the six dyes are quite comparable (comprised between 1.13 and 2.15 x 10^{-7} mole×cm^{-2}) it appears reasonable to attribute the variation of the performances to the photochromic behaviour of the dyes once incorporated in the solar cells.

To corroborate this hypothesis, we investigated the photochromic properties of semi-transparent devices. We measured the thermal discolouration kinetics of the photo-generated isomers in complete cells and measured the average visible transmittance (AVT) between 380 nm and 740 nm of the cells at the photostationary state (See **Figure 6**). The decolouration kinetics, transmittance curves and AVT values, before and after light soaking, and the light utilization efficiency values (LUE) are given in **Supplementary Table 1**.

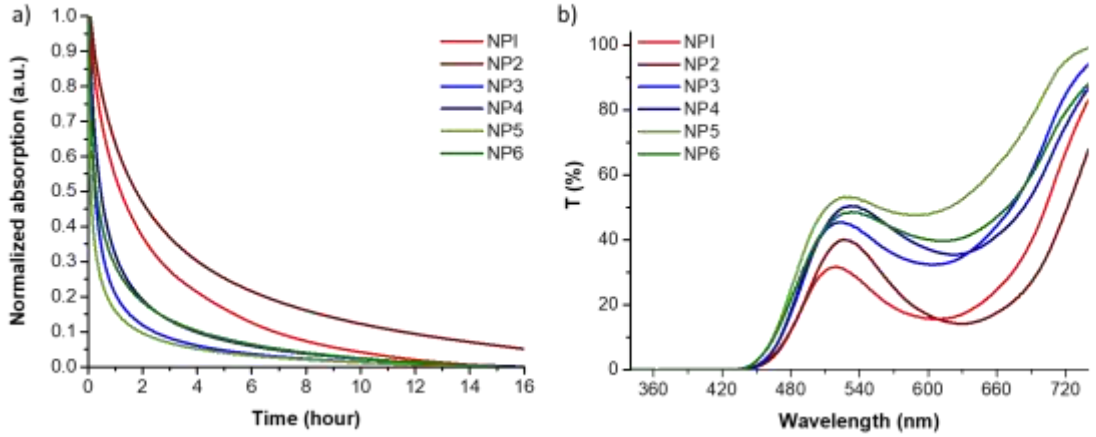

Figure 5: Optical characterization of the semi-transparent solar cells with 5 mM CDCA at 25°C a) Normalized thermal decolouration kinetic curves of **NP** dyes after reaching the photostationary state under polychromatic irradiation, b) Average visible transmittance of the **NP** dyes at irradiation at the PSS.

From these two experiments, we clearly demonstrate that the photovoltaic performances of dyes are closely related to their photochromic behaviour. Indeed, dyes that show slow thermal decolouration kinetics, such as **NP2** and **NPI** will tend to accumulate a larger amount of coloured isomers at the electrode surface under illumination. This will result in strong absorption in the visible range (low AVT at the PSS) and consequently higher J_{sc} are obtained. In contrast, dyes with faster thermal decolouration constants, induced by the steric hindrance of bridge, will tend to accumulate fewer molecules in the coloured state at the electrode surface and will therefore show less efficient absorption of photons across the visible range in the photostationary state (higher AVT at the PSS). Therefore, the J_{sc} delivered by these solar cells will be lower, and consequently the PCE is decreased. Even if it is difficult to draw clear conclusion on the evolution of the FF, we notice a trend. The introduction of bulky substituents on the indene bridge, give rise to higher FF. This may indicate that such substitution helps reducing the recombination pathways (see electrochemical impedance spectroscopy study below). Interestingly, the introduction of bulky substituents on the bridge allows for the improvement of the LUE increasing from 0.80 for **NPI** and **NP2** to values comprises between 0.99 and 1.12 for the other dyes. It should also be noted that the acceleration of the bleaching process with the introduction of bulky groups observed in solution is also observable in DSSC configuration; the fastest dye leading to a solar cell recovering 80% of its initial transparency in less than 1h.

2.4.2. How the substitution of dyes affects the V_{oc} drop upon illumination

One weakness of DSSCs sensitized with photochromic naphthopyrans is the relatively low V_{oc} of these devices (< 0.56 V). In photochromic cells, we also usually observe under irradiation a drop of up 50 mV of the V_{oc} once the PSS was reached.[43] One of the most useful techniques to gain information on transport and recombination processes in DSSCs is electrochemical impedance spectroscopy (EIS), where a small voltage modulation is superimposed on the steady-state open-circuit voltage, and the modulated current is measured.[44]–[49] In a previous study, we developed a methodology combining EIS and intensity-modulated photocurrent spectroscopy (IMPS) to study photochromic solar cells and we unravelled the origin of this V_{oc} loss. We established that the chemical capacitance of the cells remains unaltered between the dark and activated states, and that the V_{oc} drop upon illumination was solely originating from a kinetic effect that accelerates recombination when the dyes turn from their closed form into their opened form.[50]

One of the objectives of the functionalization of the **NP** dyes with alkyl chains on was to validate if such modification could lead to a better passivation of the TiO_2 surface. The modification of classical dyes with alkyl chains was often proved to reduce the recombination of electrons from TiO_2 with the electrolyte via an "umbrella" effect.[51] **Figure 6** presents the J(V) curves of opaque solar cells in the dark (black lines), then after 15s of irradiation (red lines) and at the PSS (blue lines).

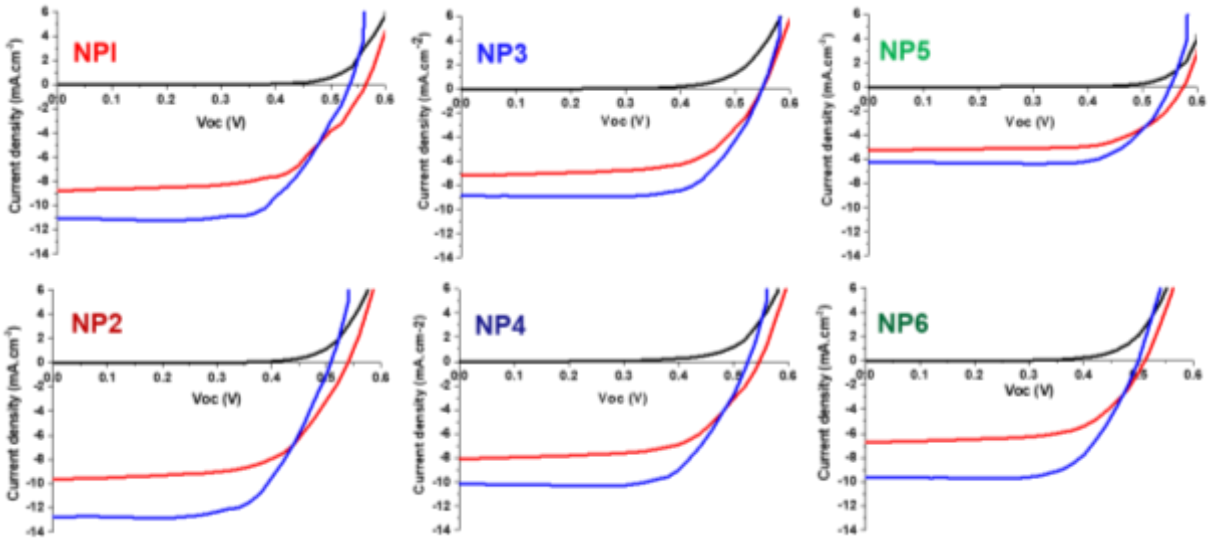

Figure 6: Current density–voltage characteristics of the opaque photochromic solar cells registered in the dark (black lines), after 15 seconds under irradiation (red lines) and after at

least 300 seconds under continuous irradiation to reach the PSS (blue lines). Standard irradiation conditions were AM 1.5 G, 1000 $W \times m^{-2}$ at 25 °C.

From **Figure 6**, it can be noted the V_{oc} difference between the first curve registered after 15s under irradiation and that at the PSS, is higher for **NPI** with a drop of 30 mV. For **NP2** the drop is 26 mV. For the dyes with bulky substituents on the indene bridge, *i.e* **NP4**, **NP5** and **NP6** the magnitude of the V_{oc} drop is 21 mV, 24 mV and 19 mV respectively. Distinctively, with **NP3**-based solar cells, this drop is not observed and V_{oc} remains constant (or even sometimes slightly increased) with irradiation time. Therefore, these differences between dyes may be indicative of a passivation effect of the alkyl chains that help decreasing the recombination rate. To verify this hypothesis, EIS experiments were carried out on the solar cells before and after activation of the dyes. Dark condition measurements were done after fabricating the cells in nearly dark conditions and storing the cells overnight prior to the measurement to ensure that they were completely deactivated and only the closed form existed. On the other hand, measurements done under illumination were taken after 15 minutes of continuous light soaking while carrying out the J(V) curves to a constant efficiency value, under 1 Sun, to ensure open forms are generated, and the PSS is reached. The Nyquist plots in the dark and under irradiation (at approximately the same value of the voltage) were registered using transparent solar cells, and are presented **Figure 7**.

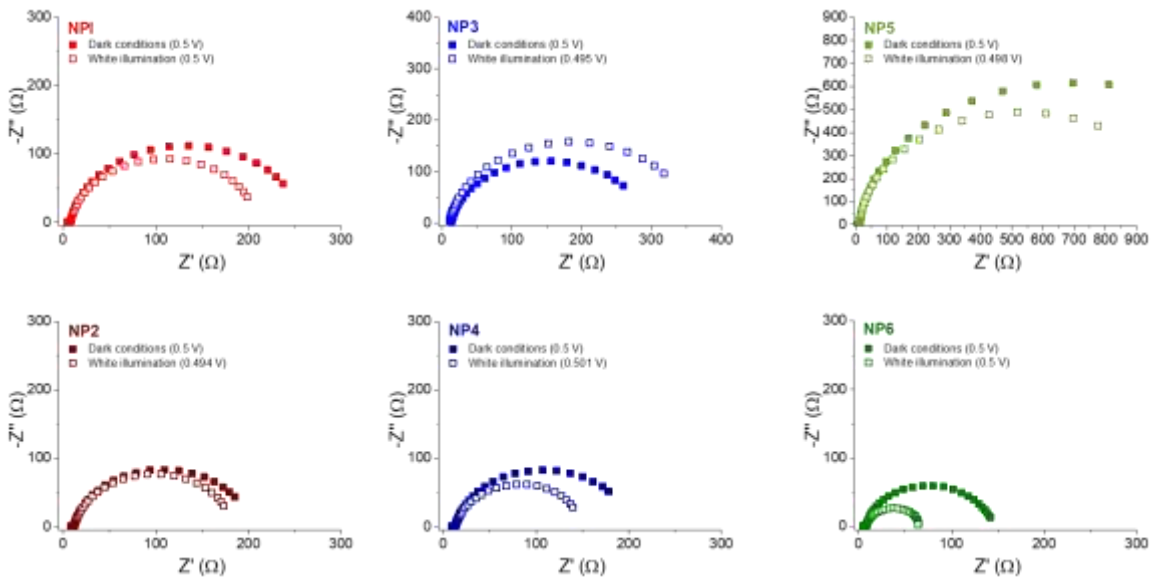

Figure 7: EIS results for **NP** dyes solar cell, the Nyquist plots are shown both before and after light soaking.

The resulting Nyquist plots include two well distinguished semicircles, one at high frequencies and the other at lower frequencies. The first one contains information on reactions in the cathode[52][53], which is beyond the scope of this work. The second signal is the most relevant for this study, and corresponds to the parallel combination of the charge transfer or recombination resistance (R_{rec}) and the chemical capacitance of electron accumulation in the semiconductor film (C_μ).[43][51][54] This second arc was fit to an equivalent –RC– circuit element, corresponding to the recombination resistance and the chemical capacitance of the device, respectively.

R_{rec} and C_μ generally show a voltage dependence[58], as can be observed in **Supplementary Figure 25**, which can be expressed using the equations below , where C_0[59][60] and R_0[48] are a pre-factors, α[58][61] is the trap distribution parameter that could help us define the average depth of trap states and hence CB alignment, β[62] is the recombination reaction order, k_B is the Boltzmann constant, and T the absolute temperature.

$$C_\mu = C_0 \exp\left(\frac{\alpha q V_{oc}}{k_B T}\right) \quad (2)$$

$$R_{rec} = R_0 \exp\left(-\frac{\beta q V}{k_B T}\right) \quad (3)$$

For all **NP** dyes, the capacitance and resistance exponential voltage dependence matches with what is usually reported for DSSCs. The values of α and β can be found in **Supplementary Table 2**. These parameters' values for all **NP** dyes remain within the usually reported values of these parameters for DSSCs[61]–[63] (0.15 – 0.35 for α and 0.5 – 0.8 for β). For the capacitances, the slopes for the different dyes are very similar, following parallel lines. When the comparison between the closed and open form of each dye is made, it can be observed that the trend lines for the capacitance dependence on voltage overlap as can be observed in **Supplementary Figure 25** and inferred from α values in **Supplementary Table 2**. The C_μ, for a given voltage, depends on the positioning of the TiO_2 CB with respect to the electrochemical potential of the redox couple. Therefore, the overlapping trendlines for the open and closed forms of each dye confirms that no CB shift occurs for this series when dyes isomerize from the closed isomer, in the dark, to an open isomer, under light. As for the β values under illumination, **NPI** and **NP2** values are slightly higher than the range mentioned above, as it has been already reported in previous works for **NPI**[19][50], the differences are not large enough to justify a change from the typical main recombination pathway for DSSCs, corresponding to triiodide reduction.

For all photochromic dye-based cells except **NP3**, the semi-circle in the dark shrinks upon exposure to irradiation at the same voltage, which is typical in classical DSSCs.[64] Such shrinks correspond to the local I_3^- concentration increase upon illumination due to dye's regeneration hence fastening recombination[45][64] accompanied with the dyes' surface isomerization that creates recombination routes. On the contrary, **NP3**-based cell shows an increase in the recombination resistance upon illumination. This is in line with the lack of V_{oc} loss as opposed to other series molecules and in some cases, a slight V_{oc} increase of up to 4 mV in transparent solar cells was observed. From this observation, we can conclude that even though the activation of the photochromic dye accelerates recombination kinetics, substitution with alkyl chains on specific position of the dye (notably on the indene bridge) helps to circumvent this phenomenon. Thus, the isomerisation of **NP3** dye and its reorganisation within the monolayer, helps to limit the local I_3^- concentration increase at the surface of TiO_2 thus lowering the recombination rate. Since electrodes from the same batch were used, any decrease/increase in charge transfer resistance is exclusively linked to the photo-isomerisation of the dyes.

With the experiments described above, we have understood the nature of recombination for **NP** dyes. To make direct quantitative comparison, it is necessary to ensure that the measurements are done at the same electron density at the photoanode.[48][60][65] Attending to the capacitance plots, parallel displacement between different cells can be observed. This behaviour suggests that the conduction band edges of the semiconductor is shifted. Thus, it is vital to apply a voltage correction to ensure that all the cells are at the same electron quasi-Fermi level (see **Figure 8**). However, this is only possible in systems with similar traps density and distribution parameter. Such corrections are done to compare recombination kinetics at the same electron density thus giving a way to distinguish thermodynamics from kinetics.[44][66][67] Since similar electrodes were applied, an assumption taken is that the NT and α are comparable hence no need for capacitance integration and that the slight differences are because of dyes' structural differences. In the dark, the capacitance plots are parallel to each other indicating the differences in the electron densities within the metal oxide (see **Supplementary Figure 25**). The same trend is observed when cells were irradiated and the dyes attained the PSS. This suggests that the conduction band edges of TiO_2 shifts in between the dyes.[59][61]

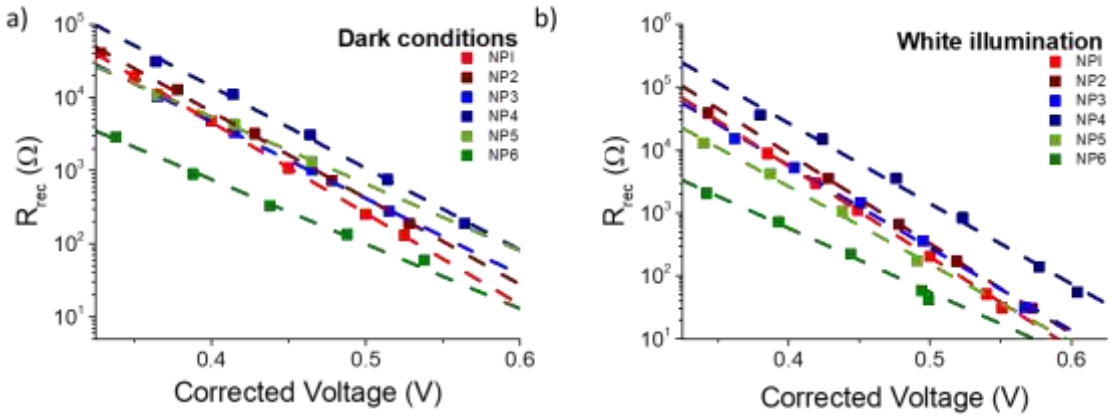

Figure 8: Evolution of the resistance of recombination for the **NP** dyes with respect to **NPI** in the dark (a) and under illumination (b).

At the same electron concentration, we were able to extract information crucial for comparison of these dyes. From **Figure 8**, it appears clearly that **NP4**, the dye bearing the highest number of hydrophobic linear alkyl chains (4 hexyls and 2 octyls), shows the highest recombination resistance under both illumination conditions. **NP2** and **NP3**, bearing 4 linear alkyl chains, show a quite similar recombination resistance which is higher compared to **NPI** especially at open-circuit potential above 500 mV. **NP6** shows the lowest recombination resistances both in the dark and under illumination in the same experimental conditions which is fully consistent with the lower V_{oc} of its cells (<500 mV) at the PSS. This analysis indicates that linear alkyl chains attached to the core of the photochromic dye have a higher passivation effect compared to branched ones and that the more the dye contains such substituents the more the recombination resistance is high.

2.5. Co-sensitization approach in photochromic DSSCs

To improve the performances of DSSCs, the co-sensitization of the electrode with multiple dyes is a simple and efficient method.[68][69] Very often, this approach resulted in record efficiencies.[70][71] Recently we demonstrated that using a blend of two benzothiadiazole-based dyes with identical pi-conjugated backbones and differing alkoxy groups on the triphenylamine unit (with CDCA as co-adsorbent) significantly improves the PCE compared to the solar cells sensitized with only one of these dyes (from 9.5% to 10.9%).[72] To the best of our knowledge, this approach was never tested yet with photochromic dyes, but the co-grafting of two of **NP** dyes may be a promising strategy to explore for improving the performances of our photochromic solar cells. We decided to focus on the combination of **NPI** and **NP2** since these

two molecules lead to the highest efficiencies both in semi-transparent and opaque cells when studied individually.

The co-sensitized DSSCs were fabricated using dyeing baths containing 0.5 mM of a mixture of **NPI**/**NP2** with ratio of 1/3, 1/1, and 3/1 in presence of the same amount of CDCA (2.5 mM) for the three different combinations of dyes. For all the ratios, slightly improved performances were measured compared to solar cells using only **NPI** dye (see **Supplementary Table 4**).

Notably, the photocurrent increases linearly to reach a maximum of 13.63 mA×cm^{-2} upon increasing the molar ratio of NP2 from pure **NPI** up to 1/3 mixture of **NPI**/**NP2**. On the other hand, the photovoltage remains nearly constant for all blends except with the blend ratio 1/1 possibly due to better surface passivation and organization of the dyes. As a result, this optimum composition yields the best solar cell with a J_{sc} of 13.43 mA×cm^{-2}, V_{oc} of 0.52 V, and a FF of 0.62 leading to a PCE of 4.34% at the photostationary state. This improvement compared to the results using only **NPI** or **NP2** dyes is mainly due to an increase in the J_{sc}. The J(V) curve of the best performance device using the three different dye options can be found in **Figure 9**, together with absorption spectra of semi-transparent devices at PSS, while the statistics performed on three opaque cells and the J(V) characteristics are as shown in ESI **Supplementary Table 4**.

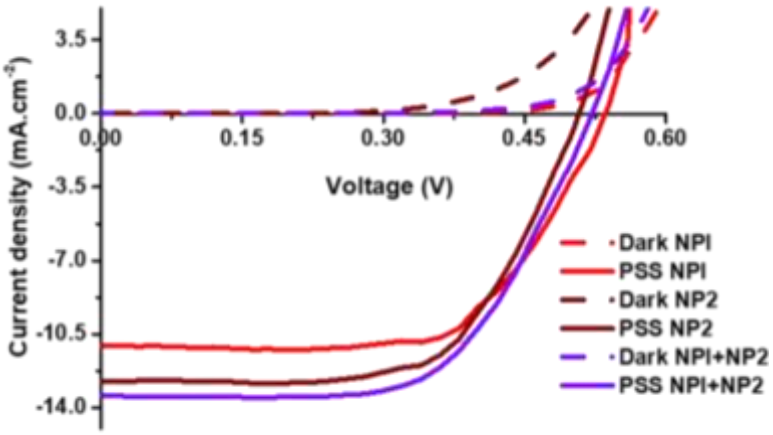

Figure 9: a) Current density–voltage characteristics of opaque photochromic solar cells (13 µm mesoporous + 3µm scattering layer) electrodes from the same batch, registered after at least 5 minutes under continuous irradiation to reach the PSS for DSSCs based on **NPI**, **NP2** and co-sensitized with **NPI+NP2** (1:1). Standard irradiation conditions were AM 1.5 G, 1000 W×m^{-2} at 25 °C.

The increase in the PCE is clearly linked to a higher J_{sc}, which is fully consistent with what is usually observed in co-sensitized solar cells. The increase in J_{sc} is often attributed to a broadening of the absorption range and a higher dye loading.[73][74] To cast light on the effect of the co-sensitization in the optoelectronic properties of the device, an EIS study was conducted on the three types of devices. The typical shrink of the semicircle upon illumination in the Nyquist plot[64] of a co-sensitized **NPI+NP2** cell can be observed (see **Supplementary Figure 26**). This behaviour is similar to what was observed for the cells using **NPI** and **NP2** only, as depicted in **Figure 7**. These spectra can be fit using the same –RC– circuit element mentioned previously, and the resulting resistances and capacitances show the same exponential behaviour following equations 2 and 3, respectively. The extracted resistances and capacitances for the co-sensitized DSSC can be compared to the results obtained for the **NPI** and **NP2** dyes in **Figure 10** under dark conditions and using white light.

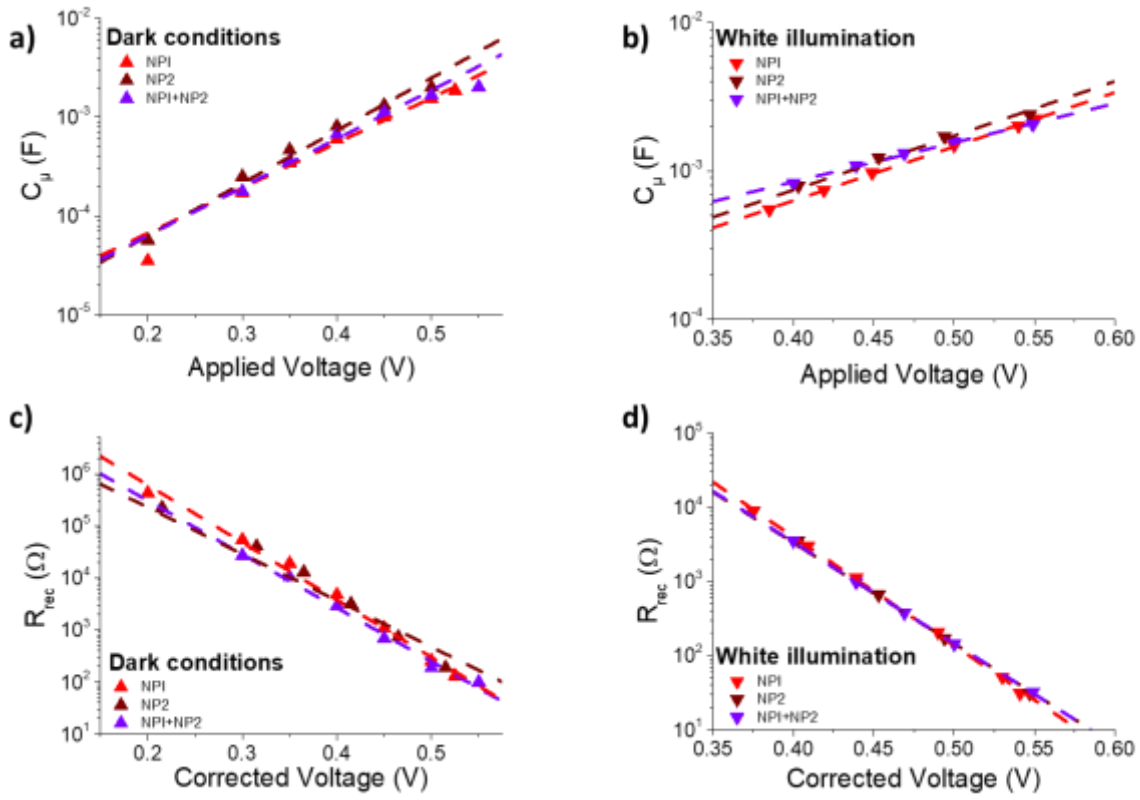

Figure 10: Chemical capacitance (a, b) and recombination resistance (c, d) vs voltage for **NPI**, **NP2** and co-sensitized **NPI+NP2** dyes under dark conditions (a, c) and white illumination (b, d). The results were obtained from fitting the main arcs of the spectra to a parallel –RC– circuit. Fits to equations 2 and 3 are included as dashed lines.

As observed **in Figure 10**, regarding the impedance, the co-sensitized dye solar cell shows similar properties to the other two dyes when used alone. The identical slopes of the trend lines observed for the three different DSSCs explain why all of them exhibit similar FF. In addition, the absence of band shift and the similar values obtained for the recombination resistance confirms the minimal impact of the co-sensitization in the V_{oc}, as can be observed in the statistical data in **Supplementary Table 4**.

Finally, we fabricated semi-transparent solar cells using the optimum dyes ratio to co-sensitize the electrodes and obtained for this composition a device with a J_{sc} of 12.26 $mA \times cm^{-2}$, V_{oc} of 0.505 V, and a FF of 0.63 leading to a maximum PCE of 3.91% at the photostationary state and a mean value of 3.87% over three devices. The best solar cell shows an AVT of 22.5% and a colour-rendering index of 65.4% giving also a LUE of 0.9. Overall, these results prove that the use of this approach to obtain higher performing devices is very promising and opens up new opportunities in the design of DSSCs with photodynamic optical properties.

2.6. Conclusion

In this article, we have reported a molecular engineering strategy of photochromic push-pull naphthopyrans dyes, via the substitution of alkyl groups in various/differing positions, allowing for modulation of their photochromic behaviour and photovoltaic properties in DSSCs. We have demonstrated that the introduction of the octyl chains on the diphenylamine donating group results in a bathochromic shift of the absorption spectra of the dyes whereas the introduction of bulky substituents on the indene bridge that connect the donating group to the photochromic core obtains the opposite effect. Substitution of the alkyl chains on the diphenylamine moiety tends to accelerate the thermal decolouration. However, the kinetics of discoloration are much strongly accelerated with increasing the bulkiness of the substituents attached to the indene group. These results prove that our strategy is a powerful and efficient method by which the kinetics of decolouration can be controlled without altering the colourability of the dyes at the PSS. When studied in solar cells, we show that the photovoltaic performances of these dyes are closely related to their photochromic behaviour. The dyes with a slow thermal decolouration kinetics exhibit stronger absorption in the visible range in the PSS (possibly connected to a larger amount of open form molecules) resulting in higher J_{sc}. Through an impedance spectroscopy study, we establish that linear alkyl chains attached to the core of the photochromic dyes result in higher passivation compared to branched chains and that the more the dye contains alkyl substituents the larger the recombination resistance will be. Among

the newly synthesized dyes, **NP2** leads to the highest performances with a PCE of 4.16%. We also report the first photochromic DSSC co-sensitized with two photochromic dyes (**NPI** and **NP2**) leading to a record PCE of 4.34% in opaque device and 3.91% in semi-transparent device configuration. Overall, this work proves that molecular engineering of photochromic photosensitizers is a promising strategy to design DSSCs with improved photodynamic optical properties and performances.

Supporting Information

Supporting Information is available from the Wiley Online Library or from the author.

Acknowledgements

J.L. acknowledges CEA for funding through a CFR PhD grant. R.D., V.M.M., and A.J.R.E. acknowledge the European Research Council (ERC) for funding. This work was funded under the European Union's Horizon 2020 research and innovation programme (grant agreement number 832606; project PISCO). J.A.A acknowledges the Ministerio de Ciencia e Innovación of Spain, Agencia Estatal de Investigación (AEI) and EU (FEDER) under grants PID2019-110430GB-C22 and PCI2019-111839-2 (SCALEUP). A.J.R.E. thanks the Spanish Ministry of Education, Culture and Sports for its supports via a PhD grant (FPU2017-03684) and Estancias Breves FPU 2021. R.D. thanks Dr. P. Maldivi and Dr. C. Aumaître for helpful discussions and O El-Dahshan for his help in the editing the final text.

Author's contributions

J.L and V.M.M. contributed equally to this work. J.L, Y.K, and Q.H synthesized the molecules. J.L performed the characterization of the molecules. V. M. M. fabricated, optimized and characterized the solar cells and analyzed the results. V. M. M and A. J. R. and J. A. A. performed the impedance study and the IPCE measurements, and analyzed the data. V. M.M, S. N. and A. H. fabricated and characterized the co-sensitized cells. R. D designed the materials and experiments, obtained the funding, supervised the study, analyzed the results and wrote the manuscript with the help of all the authors.

Received: ((will be filled in by the editorial staff)); Revised: ((will be filled in by the editorial staff)) Published online: ((will be filled in by the editorial staff))

References

[1] A. Fakharuddin, R. Jose, T.M. Brown, F. Fabregat-Santiago, J. Bisquert, *Energy Environ. Sci.* **2014**, *7*, 3952.

[2] H. Min, D.Y. Lee, J. Kim, G. Kim, K.S. Lee, J. Kim, M.J. Paik, Y.K. Kim, K.S. Kim, M.G. Kim, T.J. Shin, S. Il Seok, *Nature* **2021**, *598*, 444.

[3] Y. Cui, Y. Xu, H. Yao, P. Bi, L. Hong, J. Zhang, Y. Zu, T. Zhang, J. Qin, J. Ren, Z. Chen, C. He, X. Hao, Z. Wei, J. Hou, *Advanced Materials* **2021**, *33*, 2102420.

[4] D. Zhang, M. Stojanovic, Y. Ren, Y. Cao, F.T. Eickemeyer, E. Socie, N. Vlachopoulos, J.-E. Moser, S.M. Zakeeruddin, A. Hagfeldt, M. Grätzel, *Nat Commun* **2021**, *12*, 1777.

[5] O. Almora, D. Baran, G.C. Bazan, C. Berger, C.I. Cabrera, K.R. Catchpole, S. Erten-Ela, F. Guo, J. Hauch, A.W.Y. Ho-Baillie, T.J. Jacobsson, R.A.J. Janssen, T. Kirchartz, N. Kopidakis, Y. Li, M.A. Loi, R.R. Lunt, X. Mathew, M.D. McGehee, J. Min, D.B. Mitzi, M.K. Nazeeruddin, J. Nelson, A.F. Nogueira, U.W. Paetzold, N.-G. Park, B.P. Rand, U. Rau, H.J. Snaith, E. Unger, L. Vaillant-Roca, H.-L. Yip, C.J. Brabec, *Advanced Energy Materials* **2021**, *11*, 2002774.

[6] S. Yoon, S. Tak, J. Kim, Y. Jun, K. Kang, J. Park, *Building and Environment* **2011**, *46*, 1899.

[7] J.A. Hollingsworth, E. Ravishankar, B. O'Connor, J.X. Johnson, J.F. DeCarolis, *Journal of Industrial Ecology* **2020**, *24*, 234.

[8] Q. Xue, R. Xia, C.J. Brabec, H.-L. Yip, *Energy Environ. Sci.* **2018**, *11*, 1688.

[9] C.J. Traverse, R. Pandey, M.C. Barr, R.R. Lunt, *Nat Energy* **2017**, *2*, 849.

[10] S. Lie, A. Bruno, L.H. Wong, L. Etgar, *ACS Appl. Mater. Interfaces* **2022**, *14*, 11339.

[11] Y. Li, G. Xu, C. Cui, Y. Li, *Advanced Energy Materials* **2018**, *8*, 1701791.

[12] G.E. Eperon, V.M. Burlakov, A. Goriely, H.J. Snaith, *ACS Nano* **2014**, *8*, 591.

[13] E. Della Gaspera, Y. Peng, Q. Hou, L. Spiccia, U. Bach, J.J. Jasieniak, Y.-B. Cheng, *Nano Energy* **2015**, *13*, 249.

[14] J. Sun, J.J. Jasieniak, *J. Phys. D: Appl. Phys.* **2017**, *50*, 093001.

[15] V.V. Brus, J. Lee, B.R. Luginbuhl, S.-J. Ko, G.C. Bazan, T.-Q. Nguyen, *Advanced Materials* **2019**, *31*, 1900904.

[16] F. Grifoni, M. Bonomo, W. Naim, N. Barbero, T. Alnasser, I. Dzeba, M. Giordano, A. Tsaturyan, M. Urbani, T. Torres, C. Barolo, F. Sauvage, *Advanced Energy Materials* **2021**, *11*, 2101598.

[17] W. Naim, V. Novelli, I. Nikolinakos, N. Barbero, I. Dzeba, F. Grifoni, Y. Ren, T. Alnasser, A. Velardo, R. Borrelli, S. Haacke, S.M. Zakeeruddin, M. Graetzel, C. Barolo, F. Sauvage, *JACS Au* **2021**, *1*, 409.

[18] A.J. Lopez-Garcia, A. Bauer, R. Fonoll Rubio, D. Payno, Z. Jehl Li-Kao, S. Kazim, D. Hariskos, V. Izquierdo-Roca, E. Saucedo, A. Pérez-Rodríguez, *Solar RRL* **2020**, *4*, 2000470.

[19] Q. Huaulmé, V.M. Mwalukuku, D. Joly, J. Liotier, Y. Kervella, P. Maldivi, S. Narbey, F. Oswald, A.J. Riquelme, J.A. Anta, R. Demadrille, *Nat Energy* **2020**, *5*, 468.

[20] G.B. Van, *Photochromic Indeno-Fused Naphthopyrans*, **1997**, US5645767A.

[21] N. Rebiere, C. Moustrou, M. Meyer, A. Samat, R. Guglielmetti, J.-C. Micheau, J. Aubard, *Journal of Physical Organic Chemistry* **2000**, *13*, 523.

[22] R. Guglielmetti, **2003**, 314.

[23] B.V. Gemert, A. Kumar, D.B. Knowles, *Molecular Crystals and Liquid Crystals Science and Technology. Section A. Molecular Crystals and Liquid Crystals* **1997**, *297*, 131.

[24] S. Delbaere, B. Luccioni-Houze, C. Bochu, Y. Teral, M. Campredon, G. Vermeersch, *J. Chem. Soc., Perkin Trans. 2* **1998**, 1153.

[25] D. Venec, S. Delbaere, J.C. Micheau, M. Frigoli, C. Moustrou, A. Samat, G. Vermeersch, *Journal of Photochemistry and Photobiology A: Chemistry* **2006**, *181*, 174.

[26] C.M. Sousa, J. Berthet, S. Delbaere, P.J. Coelho, *Dyes and Pigments* **2019**, *169*, 118.
[27] M. Frigoli, J. Marrot, P.L. Gentili, D. Jacquemin, M. Vagnini, D. Pannacci, F. Ortica, *ChemPhysChem* **2015**, *16*, 2447.
[28] Z. Ning, H. Tian, *Chem. Commun.* **2009**, 5483.
[29] H. Song, X. Li, H. Ågren, Y. Xie, *Dyes and Pigments* **2017**, *137*, 421.
[30] Y. Inagaki, Y. Kobayashi, K. Mutoh, J. Abe, *J. Am. Chem. Soc.* **2017**, *139*, 13429.
[31] M.M. Oliveira, M.A. Salvador, P.J. Coelho, L.M. Carvalho, *Tetrahedron* **2005**, *61*, 1681.
[32] M. Frigoli, T. Jousselin-Oba, M. Mamada, J. Marrot, A. Zangarelli, D. Pannacci, C. Adachi, F. Ortica, *Photochem. Photobiol. Sci.* **2020**, *19*, 1344.
[33] R. Demadrille, A. Rabourdin, M. Campredon, G. Giusti, *Journal of Photochemistry and Photobiology A: Chemistry* **2004**, *168*, 143.
[34] G. Boschloo, A. Hagfeldt, *Acc. Chem. Res.* **2009**, *42*, 1819.
[35] M. Grätzel, *Nature* **2001**, *414*, 338.
[36] I. Chung, B. Lee, J. He, R.P.H. Chang, M.G. Kanatzidis, *Nature* **2012**, *485*, 486.
[37] L. Zhang, J.M. Cole, *ACS Appl. Mater. Interfaces* **2014**, *6*, 15760.
[38] A. Kay, M. Graetzel, *J. Phys. Chem.* **1993**, *97*, 6272.
[39] K. Hara, M. Kurashige, Y. Dan-oh, C. Kasada, A. Shinpo, S. Suga, K. Sayama, H. Arakawa, *New J. Chem.* **2003**, *27*, 783.
[40] T. Horiuchi, H. Miura, K. Sumioka, S. Uchida, *J. Am. Chem. Soc.* **2004**, *126*, 12218.
[41] Y.-G. Lee, S. Park, W. Cho, T. Son, P. Sudhagar, J.H. Jung, S. Wooh, K. Char, Y.S. Kang, *J. Phys. Chem. C* **2012**, *116*, 6770.
[42] O. Almora, C.I. Cabrera, J. Garcia-Cerrillo, T. Kirchartz, U. Rau, C.J. Brabec, *Advanced Energy Materials* **2021**, *11*, 2100022.
[43] J. Liotier, V.M. Mwalukuku, S. Fauvel, A.J. Riquelme, J.A. Anta, P. Maldivi, R. Demadrille, *Solar RRL* **2022**, *6*, 2100929.
[44] R. Kern, R. Sastrawan, J. Ferber, R. Stangl, J. Luther, *Electrochimica Acta* **2002**, *47*, 4213.
[45] Q. Wang, J.-E. Moser, M. Grätzel, *J. Phys. Chem. B* **2005**, *109*, 14945.
[46] C. He, Z. Zheng, H. Tang, L. Zhao, F. Lu, *J. Phys. Chem. C* **2009**, *113*, 10322.
[47] E. Guillén, L.M. Peter, J.A. Anta, *J. Phys. Chem. C* **2011**, *115*, 22622.
[48] F. Fabregat-Santiago, G. Garcia-Belmonte, I. Mora-Seró, J. Bisquert, *Phys. Chem. Chem. Phys.* **2011**, *13*, 9083.
[49] D. Pitarch-Tena, T.T. Ngo, M. Vallés-Pelarda, T. Pauporté, I. Mora-Seró, *ACS Energy Lett.* **2018**, *3*, 1044.
[50] A.J. Riquelme, V.M. Mwalukuku, P. Sánchez-Fernández, J. Liotier, R. Escalante, G. Oskam, R. Demadrille, J.A. Anta, *ACS Appl. Energy Mater.* **2021**, *4*, 8941.
[51] A. Baumann, J. Watson, J.H. Delcamp, *ChemSusChem* **2020**, *13*, 283.
[52] J. Idígoras, E. Guillén, F.J. Ramos, J.A. Anta, M.K. Nazeeruddin, S. Ahmad, *J. Mater. Chem. A* **2014**, *2*, 3175.
[53] A. Hauch, A. Georg, *Electrochimica Acta* **2001**, *46*, 3457.
[54] J. Bisquert, *The Journal of Physical Chemistry B* **2002**, *106*, 325.
[55] F. Fabregat-Santiagoa, J. Bisquert, E. Palomares, S.A. Haque, J.R. Durrant, *Journal of Applied Physics* **2006**, *100*, 034510.
[56] F. Fabregat-Santiago, J. Bisquert, L. Cevey, P. Chen, M. Wang, S.M. Zakeeruddin, M. Grätzel, *Journal of the American Chemical Society* **2009**, *131*, 558.
[57] J. Bisquert, I. Mora-Sero, F. Fabregat-Santiago, *ChemElectroChem* **2013**, n/a.
[58] J. Bisquert, *Physical Chemistry Chemical Physics* **2003**, *5*, 5360.
[59] S.R. Raga, E.M. Barea, F. Fabregat-Santiago, *The Journal of Physical Chemistry Letters* **2012**, *3*, 1629.

[60] D. Pourjafari, D. Reyes-Coronado, A. Vega-Poot, R. Escalante, D. Kirkconnell-Reyes, R. García-Rodríguez, J.A. Anta, G. Oskam, *J. Phys. Chem. C* **2018**, *122*, 14277.
[61] J.R. Jennings, A. Ghicov, L.M. Peter, P. Schmuki, A.B. Walker, *Journal of the American Ceramic Society* **2008**, *130*, 13364.
[62] J. Bisquert, I. Mora-Seró, *The Journal of Physical Chemistry Letters* **2010**, *1*, 450.
[63] J. Bisquert, A. Zaban, P. Salvador, *Journal of Physical Chemistry B* **2002**, *106*, 8774.
[64] Q. Wang, S. Ito, M. Grätzel, F. Fabregat-Santiago, I. Mora-Seró, J. Bisquert, T. Bessho, H. Imai, *J. Phys. Chem. B* **2006**, *110*, 25210.
[65] L.M. Peter, *J. Phys. Chem. C* **2007**, *111*, 6601.
[66] J. Idígoras, L. Pellejà, E. Palomares, J.A. Anta, *J. Phys. Chem. C* **2014**, *118*, 3878.
[67] Y. Kusumawati, M. Hosni, M.A. Martoprawiro, S. Cassaignon, Th. Pauporté, *J. Phys. Chem. C* **2014**, *118*, 23459.
[68] D. Koteshwar, S. Prasanthkumar, S.P. Singh, T.H. Chowdhury, I. Bedja, A. Islam, L. Giribabu, *Mater. Chem. Front.* **2022**, *6*, 580.
[69] J. Yang, X.-L. Peng, Z.-Z. Sun, S. Feng, W.-L. Ding, H.-Y. He, Z.-S. Li, *Phys. Chem. Chem. Phys.* **2020**, *22*, 5568.
[70] J.M. Cole, G. Pepe, O.K. Al Bahri, C.B. Cooper, *Chem. Rev.* **2019**, *119*, 7279.
[71] K. Kakiage, Y. Aoyama, T. Yano, K. Oya, J. Fujisawa, M. Hanaya, *Chem. Commun.* **2015**, *51*, 15894.
[72] M. Godfroy, J. Liotier, V.M. Mwalukuku, D. Joly, Q. Huaulmé, L. Cabau, C. Aumaitre, Y. Kervella, S. Narbey, F. Oswald, E. Palomares, C.A.G. Flores, G. Oskam, R. Demadrille, *Sustainable Energy Fuels* **2021**, *5*, 144.
[73] H.M. Hilal, M.A. El Bitar Nehme, T.H. Ghaddar, *ACS Appl. Energy Mater.* **2018**, *1*, 2776.
[74] T. Hua, K. Zhang, Z.-S. Huang, L. Wang, H. Tang, H. Meier, D. Cao, *Journal of Materials Chemistry C* **2019**, *7*, 10379.

*Valid M. Mwalukuku, Johan Liotier, Antonio J. Riquelme, Yann Kervella, Quentin Huaulmé, Alix Haurez, Stéphanie Narbey, Juan Antonio Anta, and Renaud Demadrille**

Strategies to improve the photochromic properties and photovoltaic performances of naphthopyran dyes in dye-sensitized solar cells.

We report a series of diphenyl-naphthopyran photochromic photosensitizers bearing various alkyl substituents for dye-sensitized solar cells. The alkyl side-chains engineering helps to improve the speed of the decolouration of the dyes and limits the recombination processes in solar cells. We fabricated, using a combination of these dyes, photo-chromo-voltaic devices showing a maximum power conversion efficiency of 4.34%.